

# Chapter 8

## Wheel-Ground Modeling in Planetary Exploration: From Unified Simulation Frameworks Towards Heterogeneous, Multi-tier Wheel Ground Contact Simulation

Roy Lichtenheldt, Stefan Barthelmes, Fabian Buse  
and Matthias Hellerer

**Abstract** Today's growing scientific interest in extraterrestrial bodies increases the necessity of extended mobility on these objects. Thus, planetary exploration systems are facing new challenges in terms of mission planning as well as obstacle and soil traversability. In order to fit the tight schedules of space missions and to cover a large variety of environmental conditions, experimental test setups are complemented by numerical simulation models used as virtual prototypes. In this context we present an integrated simulation environment which allows for using different available contact models, ranging from simple but real-time capable approximations based on rigid-body modeling techniques up to very accurate solutions based on Discrete Element Method (DEM). The models are explained and classified for their applications. For this work, a one-point Bekker based approach (BCM) and the so-called Soil Contact Model (SCM), which is a multi-point extension of the Bekker–Wong method taking soil deformation into account, are used for further analysis. These two contact models are applied for homogeneous simulations with only one type of contact model for all wheels as well as for a heterogeneous multi-tiered simulation with different contact models for the wheels. It will be shown that the multi-tiered approach enhances the simulation result accuracy compared to the results of a homogeneous model with a low level of detail while speeding up the simulation in comparison to a homogeneous higher-tier model.

**Keywords** Wheel-ground interaction · Terramechanics · Soil contact · Multi-tier modeling · Planetary exploration

---

R. Lichtenheldt (✉) · S. Barthelmes · F. Buse · M. Hellerer  
Deutsches Zentrum für Luft- und Raumfahrt/German Aerospace Center (DLR)  
Robotics and Mechatronics Center Institute of System Dynamics and Control,  
Münchener Straße 20, 82234 Weßling, Germany  
e-mail: Roy.Lichtenheldt@DLR.de

S. Barthelmes  
e-mail: Stefan.Barthelmes@DLR.de

## 8.1 Introduction

In order to further understand the formation of planets and our solar system, planetary science requires extended mobility for the exploration of extraterrestrial bodies. Therefore, the locomotion sub-systems enabling planetary exploration are facing new challenges in terms of durability and mission planning as well as obstacle and soil traversability. Testing in the actual environmental conditions is often very expensive and time-consuming or not even possible. Additionally, environmental conditions on the site of operation are often uncertain and not well-known beforehand. To cover this large variety of parameters for optimizing the locomotion sub-system and fit the tight schedules of space missions, experimental test setups are more and more complemented by numerical simulation models.

In this context we present the DLR Rover Simulation Toolkit (RST) which is an integrated simulation environment dedicated to the design of planetary rovers. For the wheel-ground contact, the RST uses an in-house developed Contact Dynamics Library (CDL) with a unified interface and modular design. This enables a straight forward implementation of rover locomotion system models including seamless switching between contact models with very different level of detail. The contact models range from simple but real-time capable approximations based on rigid-body modeling techniques via penetration and soil deformation approaches to very accurate but slow particle-based methods. Having these different techniques available in one environment allows us to directly compare results of different tier models amongst each other. Furthermore, running different contact models within one locomotion system model, which we call *heterogeneous simulations*, is exploited in this work. Our in-house Soil Contact Model (SCM), which was previously verified in [1], is the highest tier model that is still computationally efficient enough to use it in multi-body dynamics simulations. It is thus used as reference for the comparison of homogeneous lower-tier and multi-tiered heterogeneous wheel ground contacts in this work. A first feasibility study of this method was carried out in [2] and is the basis for this work. In this chapter the description of the framework and the contact models is enlarged. Due to changes in the contact detection, the expected time savings are accomplished and furthermore an in-depth analysis of new simulation results is conducted with an improved scenario.

The simulation framework is presented in Sect. 8.2. Details of the different contact models as well as a comprehensive comparison of their capabilities and applicability are given in Sect. 8.3. Heterogeneous contact modeling is the main idea of this work and is presented in Sect. 8.4. Alongside the explanation of the approach, a description of the virtual test setup used for evaluation is given. Simulation results and their discussion are shown in Sect. 8.5.

## 8.2 The DLR Rover Simulation Toolkit (RST) for Modelica

Modelica is a multi-physics, object oriented modeling language [3]. Base objects in multiple physical domains are defined by equations and interfaces, which more detailed components such as specific motors or mechanical parts can inherit from. This enables the modularity that is essential for the core part of this work while the numerous types of base objects enable modeling and subsequent simulation of complex multi-physics systems.

The RST is a Modelica library covering all relevant physical subsystems of a planetary rover, such as drivetrains, sensors and electrical systems. As shown in Fig. 8.1, other custom or commercial libraries like the DLR Visualization Library [4] are used together with RST components.

As the RST is especially focused on the locomotion and in particular on the wheel-ground contact, a dedicated Contact Dynamics Library (CDL) is used. This custom in-house library contains contact models with very different capabilities and applications which are described in more detail in Sect. 8.3. The contact models have a common interface (cf. Fig. 8.1), i.e. they require the position, velocities and orientation from the multi-body system (MBS) and respond with resulting forces and

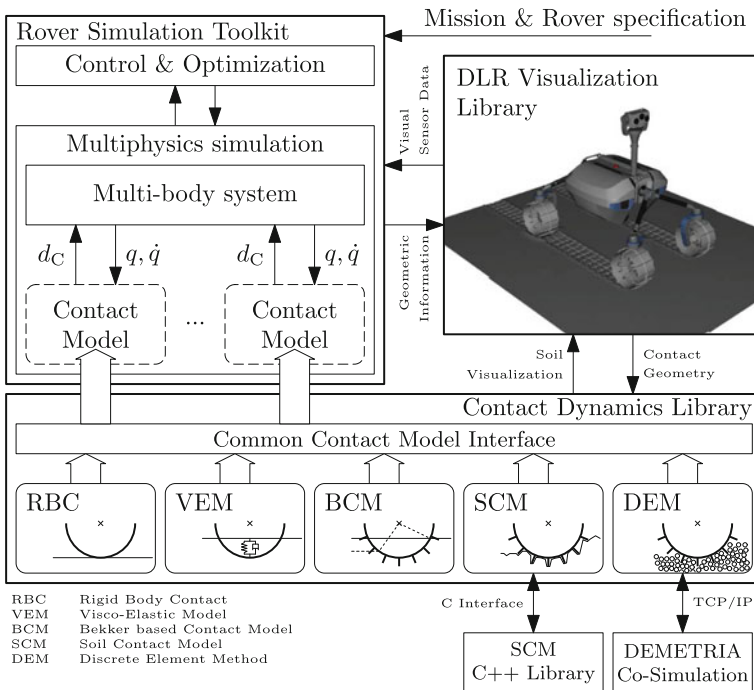


**Fig. 8.1** Structure chart of the overall simulation framework, showing the interaction between its different parts

torques. The use of the CDL transfers its variability in contact modeling for different applications to the RST. These applications comprise but are not limited to high level mission demonstration, optimization of kinematic aspects, phase 0/A studies (cf. European Cooperation for Space Standardization) for planetary exploration missions, simulation-based forensic engineering, controller design and Hardware-/Software-in-the-loop (SIL/HIL) simulations.

### 8.3 Wheel-Ground Contact Models

In this section the wheel-ground contact models included in the Contact Dynamics Library (CDL) are presented and their main features, applications as well as advances compared to the state of the art are shown. In the end of the section a systematic comparison of the models with respect to typical simulation tasks in planetary exploration is given.

#### 8.3.1 *Rigid Body Contact—RBC*

The simplest simulations of multi-body systems in conjunction with contact dynamics are typically based on rigid bodies only. While neglecting many effects of real world objects, the results are still sufficiently accurate for many applications focusing on the body movement. The big advantage of this approach is the short simulation time required: with modern desktop computers even large and complex contact scenarios can be simulated in real-time.

#### 8.3.2 *Methods*

A rigid body is defined as an idealized, perfectly non-deformable object, independent of the external forces acting upon it. General constrained connections, joints and contacts always maintain their imposed constraints and hard impacts between objects cause instantaneous object speed changes to avoid any penetration. In reality the contact between two hard objects deforms both objects, even if only slightly, for a very short time before they flex back to their original form, separating the two objects. Since this effect happens within such a very short period of time, one might only be interested in the result of this contact, namely the change to the objects movement, due to the contact.

For a rigid body simulation only the impulse of a contact, is calculated and then reapplied to the objects, thereby instantaneously changing their velocity. For further details refer to [5–7]. This principle may be used to directly calculate the speed of the

two objects, right after a collision happened between them, according to the *Impulse based collision law*, modeling the dissipation by the *coefficient of restitution*.

The *coefficient of restitution*  $\varepsilon \in [0, 1]$  depends on the material of the two objects involved. A value of 0 is called a perfect inelastic collision, a value of 1 corresponds to the perfect elastic collision.

Persistent contacts are modeled, similar to joints, as constraints on the possible relative movement. However, they only limit the movement in one direction. This is typically formulated as a *Linear Complementarity Problem* [8]:

$$\mu = A\lambda + b \quad (8.1)$$

$$\mu_i \geq 0 \quad \forall i \quad (8.2)$$

$$\lambda_i \geq 0 \quad \forall i \quad (8.3)$$

$$0 = \sum_i \mu_i \lambda_i \quad (8.4)$$

$$\mu, \lambda, b \in \mathbb{R}^n; A \in \mathbb{R}^{n \times n}; i \in [1, n]_{\mathbb{N}}$$

Applied to the contact modeling this means: either the relative force is larger than zero and the relative acceleration is zero, that is when the object surfaces are in touch, or the relative acceleration is larger than zero and the relative force is zero, when the objects are separating [9].

While dynamic friction may easily be incorporated into this approach as a force acting against the relative tangential motion of the objects, static friction is more challenging. The most common solution to this, and the one implemented here, is an approximation of the friction cone by a symmetric polyhedron [7].

### 8.3.3 Application

Rigid body models are one of the simulation techniques used most often in the computer animation and gaming industry. However, for scientific simulations its accuracy imposes certain limitations that need to be considered.

In the context of wheel ground contact simulations this technique is not applicable to the contact with soft soil, yet it is well suited for the contact between rigid wheels and a hard surfaces. In a heterogeneous simulation environment, the high computational efficiency of this model can therefore be used to quickly simulate the contact of wheels with stones in the ground.

### 8.3.4 Visco-Elastic Model—VEM

The foundation of the Visco-elastic model is that at the single point of collision a virtual spring-damper—also named KELVIN-element—is introduced. By attaching the spring-damper to the contact points of the overlapping bodies, deformation imposed forces are modeled. The difference between the non-penetrating rigid-body model and this penetration-based model is depicted in Fig. 8.2.

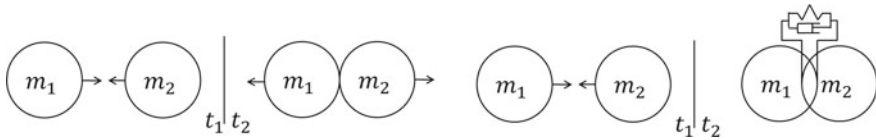


**Fig. 8.2** Rigid-Body model and penetration model for Wheel-ground contact simulations—*Left side* impulse transfer, *right side* virtual spring damper elements

### 8.3.5 State of the art

In many non-scientific applications this approach is used with spring-damper parameters that are not representative for the objects involved but rather chosen in a way that the result gives a qualitative agreement to reality while maintaining numerical stability at larger time steps. Obviously this scaling approach is not suitable for a scientific simulation [9]. Besides a physical parameterization, more complex and realistic simulations may also incorporate the penetration volume and non-linear spring-damper characteristics (cf. [10]).

For the accurate modeling of real objects, sufficiently high spring and damper constants are required. During the simulation of several stiff bodies colliding, a very small integration time-step is required for the numerical stability of the resulting stiff system. Even for unconditionally stable integration schemes the penetration change during one step can lead to extremely high separating forces during the next step, causing unrealistic behavior if the time-steps are too large [7].

### 8.3.6 Methods

In the Contact Dynamics Library we use a spring-damper element based on penetration depth which can either be configured as a linear spring and damper or non-linearly based on Bekker's parameters (cf. Sect. 8.3.8) at critical damping in conjunction with LEHR's damping fraction. For the tangential contact force a COULOMB friction model

with optional static friction based on a non-linear function of the relative movement speed is implemented. This approach avoids the need for the common regularization using further KELVIN elements. The contact detection is based on the DLR Visualization Library and uses the same contact detection technique as shown in Sect. 8.3.8.

### **8.3.7 Application**

Visco-Elastic models are popular where the simulated scene either isn't too complex and simulation speed is crucial or wherever the detailed evolution of contact forces is a required result and simulation time does not matter. Sufficient computational speed is achieved as long as the configuration is not too stiff as described in Sect. 8.3.4. The results are typically more accurate than those of the rigid-body simulation, especially if at least one of the involved bodies is comparatively soft. If realistic stiffness values are used in conjunction with non-linear spring-damper elements, high accuracy can be achieved by sacrificing computational efficiency [11]. The model is neither based on terramechanic considerations nor on impulse exchange, hence it is not the first choice for wheel-soil interaction focused simulations. However, with the correct parameterization this method can be used for some applications e.g. mission scenario demonstration to simulate both the hard contacts of wheels with rocks and for soft soil contacts maintaining a certain limited sinkage. For such applications the accuracy may be sufficient and its computational efficiency makes it a reasonable choice.

### **8.3.8 Bekker Based Contact Model—BCM**

The main idea of the Bekker based Contact Model (BCM) is to provide the fundamental terramechanical effects on soft, sandy soils with low computational effort. The contact forces and torques are computed based on a single wheel reference point and a plane describing the contact situation to the actual surface. The wheel is solely described by a set of geometrical parameters, i.e. no point cloud or surface model is used. By applying the well known Bekker–Wong theory [15], BCM can be used in scenarios where specialized terramechanical effects like rutting or multipass can be neglected but effects like the sinkage behavior, slip or the maximum traction force cannot.

### **8.3.9 State of the art**

Bekker's base model is best known for its role in the design of the Lunar Roving Vehicle [12], but has found popularity in the development of planetary exploration rovers. A similar implementation, a part of the ARTEMIS (Adams-based Rover

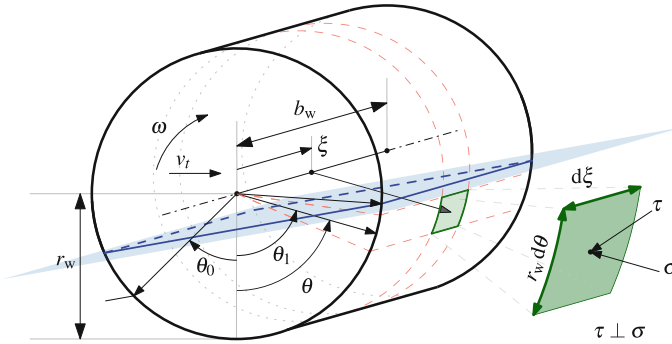


**Fig. 8.3** Concept of BCM with an infinitesimal contact patch in green, the estimated soil plane in blue, the forward  $\theta_1$  and backward  $\theta_0$  contact angle as well as the control variables  $\theta \in [\theta_0, \theta_1]$  and  $\xi \in [0, b_w]$

Terramechanics and Mobility Interaction Simulator), was presented by Trease and the group of Iagnemma [13, 14]. The shown implementation was used to analyze the MER (Mars Exploration Rover) mobility. Like BCM these models are mainly based on the semi-empirical relations developed by Bekker in the 1950s with modification by [15]. Since Bekker's theory only describes the relation between sinkage and normal pressure it is commonly combined with Janosi and Hanamoto's extensions to Mohr–Coulomb failure criterion which is also described in [15].

### 8.3.10 Methods

In BCM the reaction forces and torques are calculated by evaluating the resulting normal and shear stress for single contact patches on the wheel surface in relation to the simplified soil plane (Fig. 8.3). Additionally, force reactions on the grouser faces and tips as well as the wheel sides are considered.

The soil is described by the Bekker parameters  $n$ ,  $k_c$ ,  $k_\phi$ , the angle of internal friction  $\phi$ , the macroscopic cohesion  $c$ , its bulk density  $\rho$  as well as three BCM specific parameters:  $V_j$  used in the Janosi–Hanamoto implementation of the shear stress and  $\eta$ ,  $V_\theta$  describing the contact geometry and its velocity dependency. The wheel is described by the radius  $r_w$ , width  $b_w$ , the grouser number  $n_g$  and height  $h_g$ .

BCM assumes an exponential reduction of the backward contact angle  $\theta_0$  with a maximum reduction of  $\|\theta_0\| = \eta \|\theta_1\|$  (see Fig. 8.3). The assumed contact area spanned by  $[\theta_0, \theta_1] \times [0, b_w]$  is divided into smaller patches of the size  $A = r_w d\theta d\xi$ . The total reaction force and torque is calculated by integrating over  $\theta$  and  $\xi$ . The normal pressure  $\sigma$  acting on each contact patch is based on Bekker pressure sinkage relation [15] with  $b$  being equivalent to the wheel width  $b_w$ .



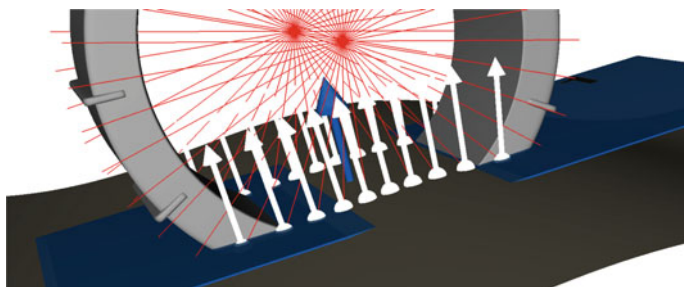


**Fig. 8.4** Contact plane estimation in BCM implemented using the line surface contact detection provided by the DLR Visualization Library. With the search direction in *red*, the detected contact points and normals in *white* as well as the estimated soil plane in *blue*

$$\sigma = \left( \frac{k_c}{b} + k_\phi \right) z^n \quad (8.5)$$

The shear stress  $\tau$  acting on each contact patch is calculated by reducing the maximum shear stress  $\tau_{\max}$

$$\tau = \tau_{\max} \operatorname{sgn} \left( \frac{dj}{dt} \right) \left( 1 - e^{-\|dj/dt\|/V_j} \right) \quad (8.6)$$

This shear stress ( $\tau$ )-shear velocity  $\left( \frac{dj}{dt} \right)$  relationship is derived from the shear stress ( $\tau$ )—shear displacement ( $j$ ) relationship originally developed by Janosi–Hanamoto which proposes an exponential relationship [15]. The used maximum shear stress  $\tau_{\max}$  is the result of the Mohr–Coulomb failure criterion

$$\tau_{\max} = c + \sigma \tan \phi. \quad (8.7)$$

Forces acting on grouser and the wheel sides are based on Rankine’s passive earth pressure [16]

$$\sigma_p = \gamma_s z N_\phi + q N_\phi + 2c \sqrt{N_\phi}, \quad \text{with } N_\phi = \tan^2 \left( \frac{\pi}{4} + \frac{\phi}{2} \right), \quad \gamma_s = \rho g. \quad (8.8)$$

Figure 8.4 shows a visualization of the algorithm used to reduce the contact geometry to a plane. The algorithm is based on line surface contact detection provided by the DLR Visualization Library [4]. The contact plane is fitted into the detected contact points, contact normals, and the wheel normals corresponding with the contact points using a least squares optimization.

### **8.3.11 Application**

The model is suitable wherever fast simulations covering the basic effects of terramechanics are required. Thus, it is most applicable for virtual prototyping in control, as used in the feasibility study for the DLR-SR robotic single wheel testbed [17].

### **8.3.12 Soil Contact Model—SCM**

Up to this point the soil did not actually deform. However, one very important effect for the simulation of planetary rovers is the plastic deformation of soil caused by the wheels. In our simulation framework we use the SCM (Soil Contact Model) algorithm for the simulation of soft soil contact forces and plastic deformation of the soil. SCM is a in-house developed, highly specialized, three dimensional, novel extension of the well known Bekker–Wong method based on [1, 18].

### **8.3.13 State of the Art**

Similar to BCM, SCM is based on Bekker’s theory and incorporates several extensions. In earlier implementations of SCM by Krenn [1, 18] the soil deformation was implemented similar to [19]. Another implementation of discretized Bekker model using soil deformation is shown in [13, 20]. An alternative approach to cover soil deformation in empirical soil models is shown in [21], by using locally spawned particles for the displaced soil volume.

### **8.3.14 Method**

Analogously to the previously introduced models, SCM is based on surface contacts for both wheel and soil. In contrast to the single point contact models, which use the soil surface only for contact detection, SCM calculates reaction forces and the soil deformation by mapping the wheel nodes onto a discretized soil grid. Therefore, only the soil nodes in contact with the wheel grid are used. The normal and shear stress calculations are modular. In this context a normal model based on Bekker’s theory [15] is used. The shear model uses an implementation of Mohr–Coulomb failure criterion with extensions by Janosi–Hanamoto [15].

In order to cover plastic soil deformation and thus rutting, as visualized in Fig. 8.5, the distribution of the soil displaced by the wheel is based on flow. A novel approach based on theoretical soil mechanics is used to deposit the distributed soil onto the surrounding nodes. Afterwards an erosion algorithm is applied to all modified nodes

to ensure that the angle of repose is abided. Thus, landslides induced around the wheels can be covered by SCM's plastic soil deformation.

Using this approach, SCM enables to cover the main effects of terramechanics and soil deformation, namely bulldozing, rutting, multipass and slip sinkage in the environment of multi-body dynamics in an efficient way. Therein multipass and rutting are covered mainly geometrically and were recently enhanced. While the volume of disposed soil and its strength are influenced by a plasticity parameter, the soil parameters themselves remain unchanged.

Summarizing the main features of the enhanced SCM are:

- Surface contact with arbitrarily shaped objects,
- Z-Buffer contact detection for each node,
- contact pressure calculation for node in contact,
- modular normal and shear stress models (for example using Bekker–Wong theory and Mohr–Coulomb failure criterion),
- coverage of dynamic slip sinkage,
- plastic soil deformation covered by compaction and displacement,
- soil displacement and compaction by theoretical soil mechanics, flow field and erosion algorithm,
- simultaneous contact of multiple objects,
- and parallelization.

### 8.3.15 Application

labelsec:app3

SCM has been successfully used in the simulation of planetary rovers [18] and the evaluation of its control using multi-body dynamics [22]. A first verification of the model was carried out in [18] for models of pressure sinkage tests, as well as full-system scale tests. Further validation is currently performed using the DLR-RMC single wheel test facility.

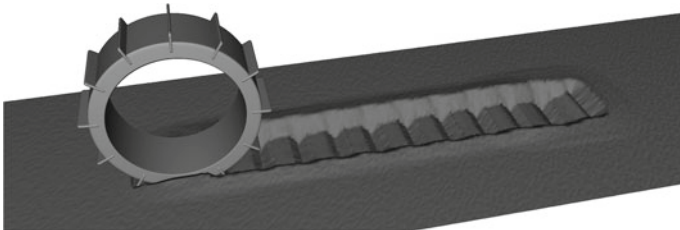


**Fig. 8.5** SCM for Wheel-ground contact simulations including terrain deformation and rutting

### 8.3.16 *Discrete Element Method—DEMETRIA*

The most detailed models are based on particle methods, i.e. the Discrete Element Method (DEM). These methods allow to model regolith directly as granular matter without the need of empirical relations.

However, even for modern powerful computers, simulations using the real grain size is still not feasible.

### 8.3.17 *State of the Art*

The Discrete Element Method (DEM) was first announced by Cundall and Strack [23]. In the recent years the method was widely adapted, improved and used by many researchers ([24–26] a.o.). In order to model real soils, the most important adaptations are the coverage of the grain shape by either complex contact geometries, e.g. [26–28] or resistance torque laws, e.g. [24, 29, 30]. Additionally, the mapping of the particle parameters to real soils was only partially solved (e.g. [24]) or carried out by calibration [28, 31, 32]. Other fields of research try to improve the computational efficiency of the method [33, 34] or deal with the calculation of hard, non-penetrating, contacts [34–36] (see also Sect. 8.3.1).

In application for planetary rover wheels, DEM has been used in order to identify influences of wheel design parameters [25], the wheel performance in lunar environment [28] or to analyze NASA's Mars Exploration Rover (MER) wheel in towed configuration [26]. Another application for wheeled vehicles is shown in [37] focused on military offroad vehicles.

### 8.3.18 *Method*

DEM is based on inter-particle contact reaction and the solution of the equations of motion for every single particle in the simulation domain. Thereby the contact laws applied are crucial for the accuracy of the simulation results. In order to allow for precise but still efficient simulations, the DLR-SR particle dynamics framework “DEMETRIA” (Discrete Element Method Enabled Terramechanics Interaction framework), based on the particle simulator Pasimodo [38], is modeling the particle shape by additional rotation geometries. By using one of these two dimensional geometries per rotation axis, an equivalent 3D rotation primitive is formed [39]. Furthermore, the framework features a systematic particle scaling and a priori parameter estimation [40] as well as dynamic boundaries. These boundaries are moved together with the tool and minimize the active number of particles by loading and deleting particles on the fly [11]. For the macroscopic contact to the wheel, the same contact laws as for inter-particle interaction are applied. However, a different parameter set is used, since the material interface is different as well. In the end, the contact reactions

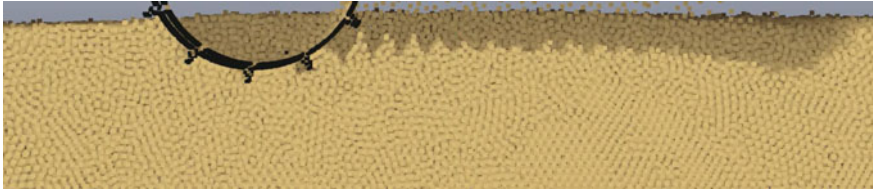


**Fig. 8.6** Wheel-soil interaction in the particle-based wheel-soil Interaction model showing principle effects of soil deformation in terramechanics

are summed up and applied to the macroscopic wheel body. For the framework's main features and advantages the reader should refer to [40–42].

### 8.3.19 Applications

DEMETRIA was successfully applied to simulation of planetary rover wheels, exemplifying running surface optimization potential [43]. The basic effects like rutting, bulldozing and dynamic sinkage, of a certain wheel surface geometry are exemplified in Fig. 8.6. Additionally, it was applied to InSight's [44] subsurface locomotion system—a self impelling nail nicknamed “the Mole”: The HP<sup>3</sup>-Mole [45] was simulated using co-simulation of particle-based soil and the MBS mechanism model [42] and influences of the outer shape on the performance were shown [46]. This co-simulation is based on TCP/IP connection between the simulators and could be used with the RST in the same way. The particle-based soil models have been verified and validated using several kinds of material tests, usually used for characterization of soils [11, 47]. In addition to that the HP<sup>3</sup>-Mole's co-simulation results are validated against deep penetration tests with an error in predicted penetration depth of less than 16% [11]. The DEM wheel models have been checked for their qualitative behaviour in worst-case soil conditions and are currently being validated using the DLR-RMC single wheel test facility.

However, due to the high demand on computation time and power, DEM is not suitable for the simulations of long trajectories at full vehicle level. Thus, these models are mainly used in order to investigate and understand the low-level effects of the interaction and thereby to enrich more efficient models. Hence the particle-based models will not be used for further investigations in this article, but are considered for future heterogeneous wheel-ground contact studies.

**Table 8.1** Comparison of used models of the Contact Dynamics Library

	Rigid body	Penetration based			
		VEM	BCM	SCM	DEM
Wheel stone contact	+ +	+	n/a	n/a	--
Wheel soft soil contact	n/a	--	--	+	+ +
Computational efficiency	+ +	+ +	+	--	--
Considered effects	--	--	+	+	+ +
Soil scalability	n/a	+ +	+ +	--	--
Multiple contacts	+ +	+ +	+ +	+ +	+
Soil deformation	n/a	n/a	n/a	+	+ +
Wheel description	S-mesh <sup>a</sup>	$r_w, b_w$	$r_w, b_w, n_{Gr}, h_{Gr}$	P-cloud <sup>b</sup>	S-mesh <sup>a</sup>
2nd body description	S-mesh <sup>a</sup>	S-mesh <sup>a</sup>	S-mesh <sup>a</sup>	E-map <sup>c</sup>	PFV <sup>d</sup>

<sup>a</sup>Surface mesh<sup>b</sup>Point cloud<sup>c</sup>Elevation map<sup>d</sup>Particle filled volume

### 8.3.20 Systematization of the Contact Models

One main advantage of the Contact Dynamics Library (models see Sects. 8.3.1–8.3.16) is that it enables easy exchange of the contact models. In order to determine which model to use for which application, a high-level overview of the models including a comparison of their characteristics is given in Table 8.1. It is pointed out that this table can only give a very general idea whereas for details the sections above need to be consulted. In typical scenarios in planetary exploration like the contact with deformable sandy soils or hard stones, each model features a certain level of detail for the application. As BCM and SCM are tailored to cover the soft soil contact only, they are not suitable for the application in wheel stone contacts. VEM and DEM are capable of covering this problem class using a different set of parameters—in both cases stones are bodies with a finite stiffness. However, rigid body approaches are most suitable for wheel stone contact, as the real deformation is negligible.

In terms of wheel sand contact, the number of considered effects is proportional with the complexity of the model. Thus DEM features the highest level of detail, due to the relocation based soil deformation. Scalability mainly depends on the discretization and dimension of the models. Thus VEM and BCM being one/two dimensional models scale best, whereas SCM and DEM being 2.5 and 3D methods slow down drastically with bigger domain sizes. Further effects add to the worse scaling behavior.

The row ‘multiple contacts’ indicates the scalability for multiple contact objects. All models but DEM scale linearly with the number of these objects. Hence, DEM is less suitable for full vehicle simulations than lower-tier methods, because of the excessive amount of computation time needed. Soil deformation is covered by the farther detailed terramechanics approaches only. Therein, SCM covers the soil defor-

mation by semi-empirical approaches, whereas DEM directly covers the deformation by grain relocation.

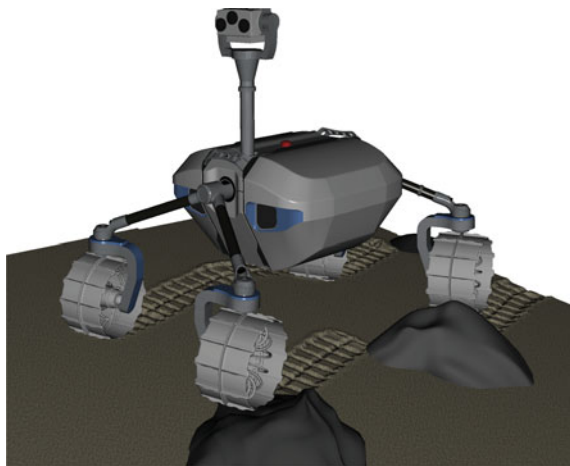
In SCM and DEM the wheel description is based on surface meshes described by vertices (nodes) and faces (elements) whereas in the other models a parametric description is used. Anyway, the surface meshes of the wheels are generated using the same parametric description, with certain limitations in terms of grouser geometry etc. for the purely parametric descriptions. The soil or general contact partner is described by surface meshes for rigid body, VEM and BCM as well. Only SCM, using equidistant and structured elevation maps and DEM using a particle filled volume described by position and orientation of each individual, are using different discretization approaches.

## 8.4 Heterogeneous Wheel-Ground Contact

The framework of the Rover Simulation Toolkit together with the Contact Dynamics Library enables using different contact models within one system model. This feature is used e.g. for the simulation of a rover traveling over sandy terrain with additional rocks embedded in the sand (cf. Fig. 8.7). For that scenario very heterogeneous contact models like SCM for the sand-contact and rigid body or the visco-elastic model for the rock-contact are used.

Besides this application which is motivated by different contact properties, a heterogeneous simulation may also be used to get a good trade-off between fast simulation and high level of detail. An example for such an approach is explained in the following and simulation results are shown in Sect. 8.5.

**Fig. 8.7** DLR-RMC Lightweight Rover Unit (LRU) [48, 49] in rough terrain, wheel-sand contact modeled with SCM, wheel-rock contact modeled with VEM



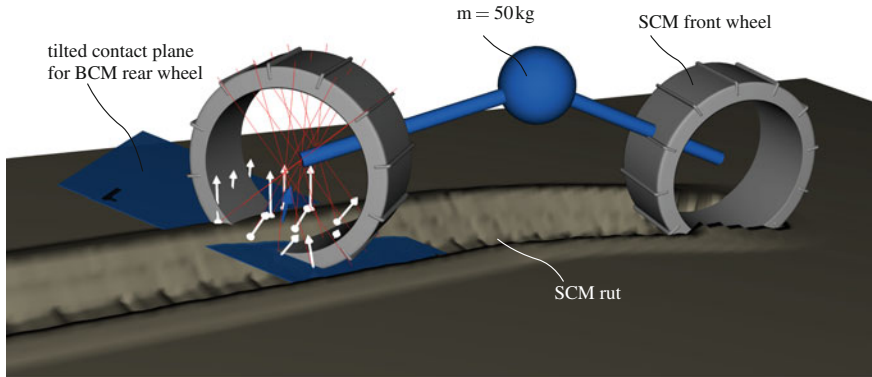


**Fig. 8.8** The test setup with BCM's contact plane detection in the SCM rut

### 8.4.1 Approach

As outlined in Sect. 8.3 and especially in the comparison in Table 8.1, different contact models have distinct capabilities and profoundly different computation times. Knowing these specifications, coupling fast and slow models can drastically improve simulation times compared to homogeneous higher-tier models with acceptable influence on the result accuracy. To achieve that, each wheel's contact model needs to cover the major individual effects of its interaction with the ground. The leading wheels of a planetary rover are usually driving through untouched and potentially loose and uncompacted soils. Thus, their model needs to not only cover the current sinkage and reaction forces, but also the soil displacement causing additional resistance due to bulldozing, as well as the generation of ruts. These ruts can lower the trailing wheel's driving resistance and at the same time apply higher lateral guidance forces. In order to cover the rutting, SCM (cf. Sect. 8.3.12) is used for the rover's leading wheels, whereas the trailing wheels are modeled one tier lower as single point Bekker (cf. Sect. 8.3.8) in order to study the approach's reasonableness. The other models presented in Sect. 8.3 will not be used in this feasibility study, but may be considered for following investigations in the field of heterogeneous wheel ground contact. Figure 8.8 shows the main effect of the proposed heterogeneous contact which is to use SCM's deformed soil for the contact detection of the trailing wheels instead of the undeformed terrain. Thereby it will be shown that the force characteristics caused by the rut of the leading wheel correspond closely to a simulation with SCM for all wheels.

The influence of the used soil simulant's compressibility on the soil parameters for the trailing wheels is neglected in this first study. Moreover, the same soil parameters are used for both SCM and BCM where applicable.



**Table 8.2** Parameters of the multi-body system, the wheel, the soil and the scenario in general

Parameter	Value
Wheel base	0.6 m
Location of point mass	10 cm above wheel axes (cf. Fig. 8.8)
Mass of point mass	50 kg
Free DoFs	All but the rotation about longitudinal rover axis
Rotational velocity of rear wheel steering	$[-0.8 \frac{\text{rad}}{\text{s}}, 0.8 \frac{\text{rad}}{\text{s}}]$
Rotational velocity of the wheels	$1 \frac{\text{rad}}{\text{s}}$
Wheel diameter $d_w$	250 mm
Wheel width $b_w$	125 mm
Grouser height $h_{Gr}$	10 mm
Number of grousers $n_{Gr}$	12
Mass of one wheel	2 kg
Soil density $\rho$	$1896 \frac{\text{kg}}{\text{m}^3}$
Angle of internal friction $\phi$	$36.7^\circ$
Cohesion $c$	66.5 pa
Bekker parameter <sup>1</sup> $k_c$	$-2.86 \times 10^6 (\text{N/m})^{n+1}$
Bekker parameter <sup>1</sup> $k_\phi$	$2.47 \times 10^8 (\text{N/m})^{n+2}$
Bekker parameter <sup>1</sup> $n$	2.49
Size of the soil plane	3 m × 1 m with 10 mm resolution (for SCM)

<sup>1</sup>The used Bekker parameters are the result of the fitting method described in [50] and do not necessarily directly correspond with physical soil properties

**Table 8.3** Simulation variables used for assessment and their corresponding objectives

Variable	Objective
CPU time factor $k_{CPU}$	Compare computation time
Tractive force $F_x$	Evaluate traction and its distribution on the front/rear wheel
Lateral force $F_y$	Evaluate guidance effect of the rut
z-position $z$	Evaluate the influence of the rut on the sinkage
Trajectory in the $x$ - $y$ -plane	Visualize impact of all above on the movement of the wheels

### 8.4.2 Virtual Test Setup

In this section, the test setup used for comparing the results of the different approaches in Sect. 8.5 is presented and choices and assumptions that were made are explained. Detailed parameters of the setup are given in Table 8.2 and the quantities that are used for evaluation are presented in Table 8.3.

**The multi-body system** For this study of heterogeneous wheel-ground contact modeling of a rover, we are mainly interested in effects of the rear wheels driving through ruts that were created by the front wheels. Using symmetry in conjunction with suit-

able boundary conditions we may simplify a four wheeled rover to only one front and one rear wheel which are connected by a rigid link and have a point mass located in between them (cf. blue body in Fig. 8.8). This assembly is able to move freely in all but the rotational degree of freedom about its longitudinal axis. Additionally, both wheels can be actuated, i.e. rotated about their local wheel axis and the rear wheel can be steered, i.e. rotated about its local  $z$ -Axis. The parameters can be found in Table 8.2.

**The soil** is a soil simulant for Martian regolith the so-called *MSS-D*. Its parameters were characterized using the DLR-RMC Bevameter in conjunction with the corresponding identification approach [50]. The parameter set is filed with the name RMCS-2. *MSS-D* was developed to simulate Martian regolith in terrestrial tests. Therefore, it mainly consists of fines and quartz sand. In addition to these soil parameters, both SCM and BCM feature a set of supplementary parameters which are chosen using physical and empirical assumptions. Additionally, the parameter choice made ensures comparability of the homogeneous simulations behavior. From a geometric point of view, a  $3\text{ m} \times 1\text{ m}$  plane with a mesh resolution of  $1\text{ cm} \times 1\text{ cm}$  is used for SCM and another one with a reduced mesh resolution of  $3\text{ cm} \times 3\text{ cm}$  for BCM. The latter choice has an effect for the contact plane detection in the rut of a SCM wheel, only. The different resolutions were found to ensure a good compromise between computational effort and result quality. It is pointed out that the lower soil resolution for BCM is only possible because—in contrast to SCM—the geometry is solely used for calculating the current contact plane (see Sect. 8.3.8).

**The wheels** have a cylindrical shape with twelve grousers and beyond that a smooth surface; the parameters are summarized in Table 8.2.

**The scenario** In order to investigate the effects of ruts of the leading wheel, a scenario wherein the trailing wheel enters, escapes and crosses the trajectory of the leading wheel is chosen. The traces of both wheels as well as the setup itself and the dimension in  $x$ -direction can be seen in Fig. 8.9. Therefore, the two wheels start aligned and travel with the same constant rotational velocity. Shortly after entering the rut of the leading wheel, the trailing wheel is steered with a constant rotational velocity for a short distance and thereby escapes the rut. Subsequently, the trailing wheel is steered back again, with a constant rotational velocity such that it crosses the trace of the

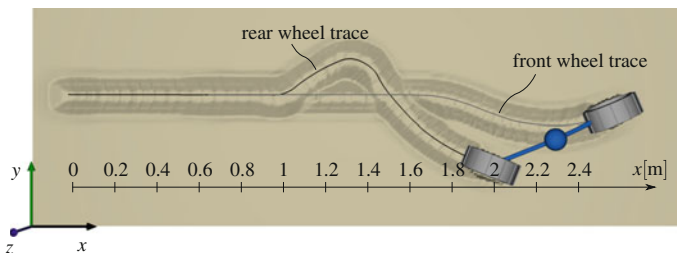


**Fig. 8.9** Traces of front and rear wheel

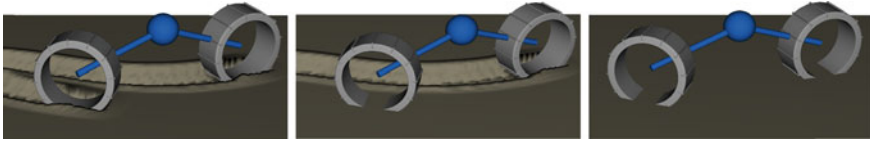


**Fig. 8.10** Virtual test scenario to evaluate the tractive performance of different rovers: SCM-SCM (*left*), Heterogeneous SCM-BCM (*middle*), BCM-BCM (*right*),

leading wheel. The timing of all steering commands in the simulation is based on position thresholds in the global  $x$ -direction of the rear wheel.

**The software** For all shown simulations, Dymola 2016 RC-2 with a development version of the DLR Visualization library [4] and the Contact Dynamics Library is used. Furthermore, an explicit 4th order Runge–Kutta fixed step solver (*rkfix4* in Dymola) with a time step size of  $\Delta t = 1$  ms is used. As the integration scheme does neither feature A-stability [51] nor step size control, the choice of the time step is constrained by the maximum eigen frequency of the system. A linearization of the contact stiffness according to Bekker’s equations (cf. Sect. 8.3.8) yields an eigen frequency of 76.5 Hz and thus a maximum time step size of 26 ms. This yields a safety factor of  $>10$  for  $\Delta t = 1$  ms. The choice of the solver itself is based on experience for a good trade-off between result quality and computational effort.

In order to check the consistency and the applicability as well as the potential speed up of the heterogeneous wheel ground contact modeling, a homogeneous simulation for each contact model is performed first. Figure 8.10 shows the single-tiered homogeneous, as well as the heterogeneous setups. For this evaluation the quantities and their respective evaluation objectives are listed in Table 8.3.

Since the objective of this work is to compare the coverage of basic terramechanics effects, the forces are normalized with respect to the maximum value of the longitudinal front wheel force of the homogeneous SCM simulation (for better readability of the plots, the force peaks at the start of the wheel rotation is not considered for this maximum value). These normalized values are noted as  $(\cdot)_0$  in the following passages. The results of the described tests are shown in Sect. 8.5.

## 8.5 Results

In this section we discuss the impact of the proposed heterogeneous contact simulations (cf. Sect. 8.4). Therefore, we compare the accuracy of the simulation results as well as the demand in computation time of the homogeneous BCM and the heterogeneous simulation to the reference homogeneous high-tier SCM simulation. The values that are used for comparison are summarized in Table 8.3. These values are common quantities for tractive performance tests in planetary rover locomotion. All

forces are plotted in a local wheel coordinate system where the  $z$ -direction is co-directional with the global  $z$ -direction. The  $x$ - and  $y$ -axes are rotated with the wheel steering angle such that the  $x$ -axis points in the wheel's longitudinal direction at all times. Note that due to this rotation the forces in  $x$ - and  $y$ -direction only sum up to zero all together (i.e. not separated in  $x$ - and  $y$ -direction) for a stationary movement. The high frequency noise observable in the SCM force is a result of the soil discretization. Due to the uniform distribution and high frequency the effects can be neglected in this context.

### 8.5.1 Detailed Description of Observed Effects in the Different Setups

The longitudinal and lateral forces as well as the  $z$ -position of all three setups are shown in Fig. 8.12, top. Thereby, the  $z$ -position denotes the position of the wheel center above the undeformed ground level. It is pointed out again that all four force plots are normalized with respect to the maximum longitudinal force of the front wheel (the peak in the beginning is not taken into account since it is not of particular interest here and would shrink the rest of the plots). The trajectories in the  $x$ - $y$ -plane of the front (solid lines) and rear (dashed line) wheels are shown in Fig. 8.12, bottom. In the following paragraphs the plotted results are explained in detail whereas a shorter overall summary of these results is given in Sect. 8.5.2. For better readability, the following abbreviations are used:

SxS homogeneous SCM model—both wheels SCM  
 BxB homogeneous BCM model—both wheels BCM  
 SxB heterogeneous model—front wheel SCM, rear wheel BCM

Also, the whole scenario can be divided into five main sections which are labeled with the letters A-E in the following and in Fig. 8.12:

- A Start of the wheel rotation and stationary driving.
- B The rear wheel enters the rut of the front wheel and subsequently drives in it.
- C The rear wheel is steered to  $\delta = 0.8$  rad and quits the rut.
- D The rear wheel is steered back to  $\delta = -0.8$  rad and crosses the rut.
- E Stationary driving of both wheels, each in its own lane.

0–0.1 m, *acceleration of the rover (A)*: There is a positive peak in front and rear wheel  $x$ -forces when the wheel starts to rotate. This is due to the correlation of high slip velocity and high shear stress. After the first 10 cm the plotted quantities seem to have reached a stationary state in all three models. However, to reach that state, SxS and SxB show a shift of the traction force to the rear wheel. This originates from dynamic wheel loading, i.e. a higher normal force on the rear wheel due to the inertia resulting from the point mass. It can also be seen that SxB transfers even more traction force to the rear wheel. This effect occurs due to the BCM simulated rear wheel being able to develop a higher traction force compared to the SCM front wheel. The latter also

shows increased bulldozing and hence lifting forces. This lifting of SCM-modeled wheels can also be seen in the  $z$ -position plot.

0.1–0.35 m, *stationary driving (A)*: All three models show a stationary condition, as rear and front forces are both almost canceled out. Looking at the  $z$ -position it can be seen that the sinkage is higher for SCM modeled wheels than for the BCM ones. This effect occurs due to differences in elastic and plastic deformation of the soil in the two models. However, the effect is beyond the scope of this work and will be subject of future research.

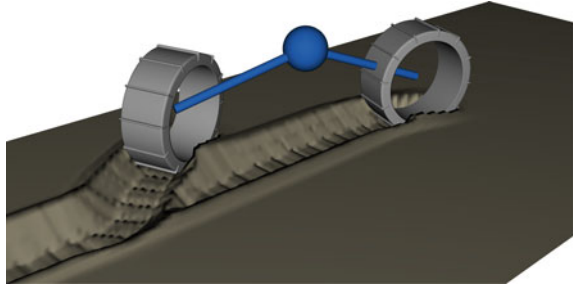
0.35–0.65 m, *rear wheel entering the rut (A-B)*: SxS and SxB both show a shift in the traction force distribution due to the rear wheel entering the rut of the front wheel. In SxS however, the rear wheel needs to traverse a bit of compacted soil first which leads to increased resistance at the rear wheel and a higher traction force at the front wheel accordingly. The BCM simulated rear wheel of SxB is able to perceive geometric changes only, which are very low for the region right before entering the rut. Hence, only SxB shows the pushing effect on the rear wheel when entering the rut. This effect can be observed in the Fig. 8.12 (top) as a shift of the tractive force to the rear wheel. By analysis of the  $z$ -position it can be seen that the rear wheel approaches the  $z$ -position of the SCM wheel by rolling down into the rut. BxB in contrast does not change from its stationary condition in any of the quantities, due to the non-existent rut of the front wheel.

0.65–0.9 m, *stationary driving in rut (B)*: The rear wheel drives stationary in the track of the front wheel. Besides the sinkage, all models deliver similar results.

0.9–1 m, *rear wheel steering (C)*: Constant steering angular velocity ( $\dot{\delta} = 0.8$  rad) until an angle of  $\delta = 45^\circ$  is reached. All models show the changing force distributions in the  $x$ - $y$ -plane, i.e. the traction force of the front wheel increases. This is compensated by a higher resistance of the rear wheel both in longitudinal ( $x$ ) and lateral ( $y$ ) direction. Note that in the first instance of steering the wheels are still almost aligned and thus no lateral force due to a steered rear wheel is exerted. Rather a small lateral force in the opposite direction of the pulling is created by the steering itself. This effect is covered by all model combinations, although SxS shows a higher magnitude of the effect. In contrast to the other models the BCM rear wheel in SxB starts to climb out of the rut, whereas the SxS rear wheel even digs in a little deeper when the steering velocity is applied. SxS's higher lateral force (cf.  $(F_y)_0$  in Fig. 8.12, top) and higher sinkage together result in a first small difference in the  $x$ - $y$ -trajectory, i.e. the SCM rear wheel shows a delay in its  $y$ -position.

1–1.1 m, *rear wheel quitting the rut (C)*: In both SxS and SxB the resistance force at the rear wheel increases because it needs to drive out of the rut. In contrast, BxB's forces remain at the level that is given by a pure geometric correlation. To be more precise, the force distribution of longitudinal and lateral forces of front and rear wheel are given solely by the steering angles of front and rear wheel. The BCM rear wheel of SxB continues climbing out of the rut and reaches an even higher  $z$ -position than for BxB which is caused by the piled soil around the SCM front wheel's rut. However, since the SxB rear wheel needs to climb up the complete sidewall of the rut, it shows a stronger guidance in  $y$ -position compared to both homogeneous

**Fig. 8.11** The homogeneous SCM configuration at rear wheel position 1.2 m where it starts steering back



simulations. This effect can be observed in the  $x$ - $y$ -trajectory in Fig. 8.12 (bottom) where the rear wheel of SxB starts to diverge in the  $y$ -position from the other two.

1.1–1.2 m, *constant conditions (C)*: For this position range the forces of SxS and SxB converge towards the BxB results. However, the period of constant steering angle is not quite long enough for the former two to reach the BxB results.

1.2–1.4 m, *rear wheel steering (D)*: The rear wheel is steered back to  $\delta = -45^\circ$  with  $\dot{\delta} = -0.8 \frac{\text{rad}}{\text{s}}$  which leads to a corresponding change in the force distributions for all models. The  $z$ -position plot shows that the SxS rear wheel starts digging in as soon as the steering is applied at 1.2 m (cf. description of 0.9–1 m). As shown in the  $x$ - $y$ -trajectory plot at the corresponding position this is not due to the rut of the first wheel since the rut is not reached yet, see Fig. 8.11. Thus, this lowering in  $z$ -position is pure sinkage due to the added resistance by steering. At 1.3 m the rear wheel is aligned with the front wheel again, which can be seen in the tractive forces of front and rear wheel being close to zero for a short distance. The SxS rear wheel even continues to sink in for about 4 cm after the alignment of the wheels was reached at 1.3 m. This considerable difference in sinkage leads to major differences in the forces in [1.3 m, 1.4 m], too. It can be seen that the SxS rear wheel is experiencing an increased resistance in both lateral and longitudinal direction. In this part the SxB result is even farther apart from the reference SxS than the simpler BxB. That can be seen looking at the rear wheel of SxB, which shows even lower resistance forces than BxB. This difference can be explained using the  $z$ -position plot: The rear wheel of SxB slides down the sidewall into the rut of the SCM front wheel and pushes the front wheel.

1.4–1.6 m, *rear wheel crossing the rut (D)*: In the SxB case the rear wheel needs to climb up the steep sidewall of the rut again. Thereby, it exerts an increased guidance force which results in a significantly lower gradient of the  $x$ - $y$ -trajectory in Fig. 8.12 (bottom). The steep slope additionally causes the longitudinal resistance force being higher for this case. All together this leads to a significantly increased traction force on the front wheel. In contrast to that behavior, SxS starts to overcome the rather high force shift of its rear wheel that was explained above. As soon as the front wheel rut is reached, the rear wheel is driving on pre-compressed soil which also supports to lower its resistance force immediately.

**Table 8.4** Factors for computation time

Model	Computation time factor
BCM	1
SCM	2.3
Heterogeneous	1.5

>1.6 m, *stationary driving (E)*: All three setups reach a similar stationary force distribution. Due to the differences described above, the trajectories continue to deteriorate. I.e. the whole rover steering angle of SxB is shifted compared to the homogeneous simulations. This is mainly an effect of the higher guidance force of the front wheel's rut on the rear wheel.

The intention of the heterogeneous contact modeling is to reduce computation time while covering as many details in the simulation result as possible. Hence, additionally to the result accuracy, the computation time is compared in Table 8.4. Factors for the computation time are introduced which represent the computation time of each setup normalized with the computation time of the BxB case,  $k_{\text{CPU}}^{\text{modelX}} = t_{\text{CPU}}^{\text{modelX}} / t_{\text{CPU}}^{\text{BCM}}$ . It can be seen that SxS takes more than twice the time compared to BxB whereas the SxB time is slightly better than the mean of SxS and BxB. Compared to the results in [2], we execute our contact search for the BCM wheels on a small patch of the surface only, which is deformed by the SCM front wheel. This leads to a major speedup of the heterogeneous model as was expected in [2]. Furthermore, due to a different scenario, modified contact models and a different solver the SCM is, compared to BCM, not as slow as it was in the previous work. Also consider that the simulations shown, were computed on a standard office PC. The simulation time would probably differ for other configurations e.g. due to SCM's recently added multi-threading capabilities.

### 8.5.2 Interpretation of the Results

The detailed explanation of all observable effects is given in Sect. 8.5.1, this short section is intended to briefly summarize the results and give an interpretation and implications for the different models/setup.

- For mission planning or similar applications where the position is the required result and variables only matter in their order of magnitude, a homogeneous BCM simulation provides adequate and sufficiently precise results. Moreover, the homogeneous BCM results for the wheel's trajectory are even closer to the reference SCM solution than the heterogeneous ones. This is caused due to the effects described after the next bullet point. Hence, the benefit of using farther detailed models for these applications should always be evaluated beforehand.
- BCM can neither model rutting of wheels nor changes in parameters for multi-pass simulation. If the effect of these ruts on the wheel forces is important, the

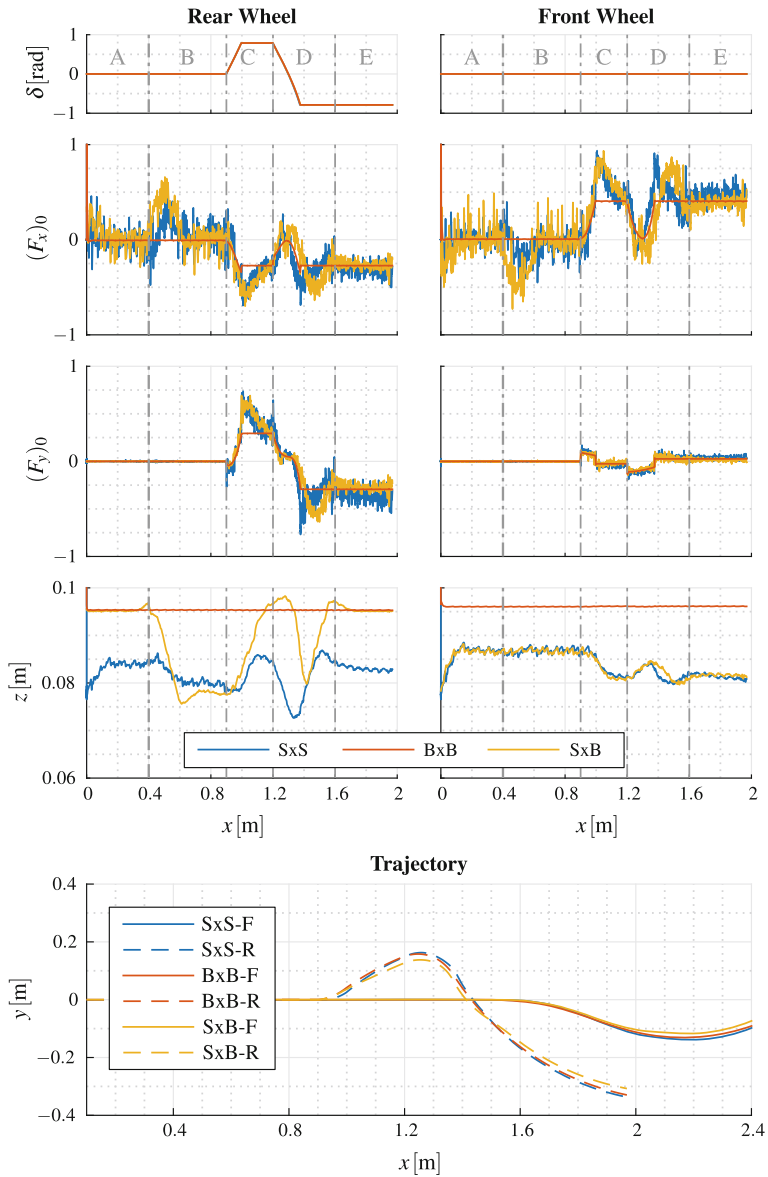


**Fig. 8.12** Forces in longitudinal and lateral direction,  $z$ -position as well as the trajectory in  $x$ -plane of the front and rear wheels. (SxS: homogeneous SCM, BxB: homogeneous BCM, SxB: heterogeneous)



heterogeneous approach offers results that are very close to a homogeneous high-tier simulation while saving a considerable amount computation time. The saved time might be crucial in many applications in planetary exploration, e.g. due to tight schedules or for simulation based forensic-engineering [52].

- The main differences between the homogeneous high-tier SCM and the heterogeneous SCM/BCM forces result from the fact that BCM or—to be more precise—its contact detection is only able to detect and react on geometrical changes of the front wheel's rut. Hence, it needs to climb comparatively large sidewalls when crossing a rut compared to SCM digging through the sidewalls. Thus SCM does not need to lift the whole rover as much as BCM.
- Independent from the scope of this work, the sinkage of BCM and SCM was found to be different by approximately 25%. This will be subject to further investigation within the currently ongoing model validation campaign using our DLR-RMC single wheel test facilities.

To conclude this section, it should be mentioned again that none of the used models has undergone a in-depth validation yet, as this is one of our currently ongoing projects. However, in this work SCM is used as a reference for two reasons: First it is partially verified by previous analysis and second it is able to cover the most effects of the two models used. Since the scope of this section is to compare the qualitative capability of modeling certain effects of wheel-soil contact using homogeneous and heterogeneous approaches and study their qualitative effects on a rover, this approach is applicable and does not require in-depth validation a-priori.

## 8.6 Conclusion

In the article we presented the integration of wheel ground contact models with different level of detail in a unified simulation framework to allow for appropriate simulation of the various tasks in planetary exploration. Furthermore, this integration enables multi-tiered heterogeneous wheel ground contact modeling in a unified manner.

By usage of our single-point (BCM) and multi-point (SCM) Bekker-based contact models this approach was exemplified in order to achieve a speed up of the simulation compared to the homogeneous higher-tier SCM model. In the chosen planetary rover locomotion scenario, the computation time was decreased considerably while maintaining almost the same level of accuracy. Additionally, drawbacks and limitations of the approach were pointed out. Due to usage of SCM deformed surface patches of limited size in BCM's contact detection the speed up of the heterogeneous model is in the expected range in contrast to the results presented in [2].

As simulants, like MSS-D, which are mainly based on fines feature excessive compressibility, a next step will be the investigation of multi-pass effects in pre-compressed ruts in compressible simulants. Additionally, further validation of the single models as well as investigations will be performed. Moreover, in order to

allow a deeper insight in the potential speed up, rovers with increasing number of wheels, featuring leading wheel's SCM contact and lower-tiered contacts for the trailing wheels, will be compared in future work. It is expected that the benefit of the increased accuracy of the soil interaction models is decreasing with a higher number of the multi-passes.

**Acknowledgments** Parts of this work have been granted by the Helmholtz-Gemeinschaft Deutscher Forschungszentren e.V. under contract number HA-304 (Robotic Exploration of Extreme Environments—ROBEX)

## References

1. Krenn R, Hirzinger G (2008) Simulation of rover locomotion on sandy terrain-modeling, verification and validation. In: 10th ESA workshop on advanced space technologies for robotics and automation—ASTRA, (2008) Noordwijk. Niederlande, ESA
2. Lichtenheldt R, Hellerer M, Barthelmes S, Buse F (2015) Heterogeneous, multi-tier wheel ground contact simulation for planetary exploration ISBN 978-84-944244-0-3
3. Elmqvist H, Mattsson SE, Otter M (1999) Modelica a language for physical system modeling, visualization and interaction. In: Proceedings of the 1999 IEEE international symposium on computer aided control system design (Cat. No.99TH8404)
4. Hellerer M, Bellmann T, Schlegel F (2014) The DLR Visualization Library Recent development and applications. In: Proceedings of the 10th international modelica conference—Lund, Sweden - Mar 10–12, 2014, pp 899–911
5. Erleben K (2004) Stable, robust, and versatile multibody dynamics animation. Phd thesis, University of Copenhagen, Denmark
6. Mirtich BV (1996) Impulse-based dynamic simulation of rigid body systems. Dissertation, University of California at Berkeley
7. Bender J, Erleben K, Trinkle JC (2014) Interactive simulation of rigid body dynamics in computer graphics. *Comput Gr Forum* 33(1):246–270
8. Cottle RW, Dantzig GB (1968) Complementary pivot theory of mathematical programming. *Linear Algebra Appl* 1(1):103–125
9. Boeing A, Bräunl T (2007) Evaluation of real-time physics simulation systems. In: Proceedings of the 5th international conference on computer graphics and interactive techniques in Australia and Southeast Asia, ACM pp 281–288
10. Marhefka DW, Orin DE (1996) Simulation of contact using a nonlinear damping model. *Proc IEEE Int Conf Robot Autom* 2(April):1662–1668
11. Lichtenheldt R, Schäfer B, Krömer O (2014) Hammering beneath the surface of mars— modeling and simulation of the impact-driven locomotion of the hp3-mole by coupling enhanced multi-body dynamics and discrete element method. In: Shaping the future by engineering: 58th Ilmenau scientific colloquium IWK, URN (Paper): <http://nbn-resolving.de/urn:nbn:de:gbv:ilm1-2014iwk-155:2> Technische Universität Ilmenau, 08–12 Sept 2014
12. Vivake Asnani, Damon Delap, Colin Creager (2009) The development of wheels for the Lunar Roving Vehicle. *J Terramech* 46(3):89–103
13. Trease B, Arvidson RE, Lindemann R, Bennett K, Feng Z, Iagnemma K, Senatore C, Van Dyke L (2011) Dynamic modeling and soil mechanics for path planning. In: Proceedings of the ASME 2011 international design engineering technical conference & computers and information in engineering conference IDETC/CIE, pp 1–11
14. Iagnemma K, Senatore C, Trease B (2011) Terramechanics modeling of Mars surface exploration rovers for simulation and parameter estimation. In: Proceedings of the IDETC/CIE 2011

- ASME international design engineering technical conferences & computers and information in engineering conference, pp 1–8
15. Wong JY (2008) Theory of ground vehicles, 4th edn. Wiley, New Jersey
  16. Terzaghi K, Peck RB, Mesri G (1996) Soil mechanics in engineering and practice. Wiley, New Jersey
  17. Fabian Buse (2015) Masterarbeit Machbarkeitsstudie für einen roboterbasierten Radprüfstand zur Entwicklung von Mars Mondrovern. Masterthesis, RWTH Aachen
  18. Krenn R, Hirzinger G (2009) SCM a soil contact model for multi-body system simulations. In: 11th European regional conference of the international society for terrain-vehicle systems–ISTVS 2009, Bremen, Germany
  19. Sumner RW, O'Brien JF, Hodgins JK (1999) Animating sand, mud, and snow. *Comput Gr Forum* 18:17–26
  20. Zhou F, Arvidson RE, Bennett K, Trease B, Lindemann R, Bellutta P, Iagnemma K, Senatore C (2014) Simulations of mars rover traverses. *J Field Robot* 31(1):141–160
  21. Holz D, Azimi A, Teichmann M, Kovacs J (2012) Mobility prediction of rovers on soft terrain: effects of wheel- and tool-induced terrain deformations. Proceedings of the fifteenth international conference on climbing and walking robots and the support technologies for mobile machines CLAWAR 2012:647–654
  22. Krenn R, Gibbesch A, Binet G, Bemporad A (2013) Model predictive traction and steering control of planetary rovers. In: 12th symposium on advanced space technologies in robotics and automation: ASTRA 2013
  23. Cundall PA, Strack ODL (1979) A discrete numerical model for granular assemblies. *Geotechnique* 29:47–65
  24. Obermayr M (2013) Prediction of load data for construction equipment using the discrete element method. PhD thesis, Universität Stuttgart
  25. Nakashima H, Oida A, Momozu M, Kawase Y, Kanamori H (2007) Parametric analysis of lugged wheel performance for a lunar microrover by means of dem. *J Terramech* 44(2): 153–162
  26. Knuth MA, Johnson JB, Hopkins MA, Sullivan RJ, Moore JM (2011) Discrete element modeling of a mars exploration rover wheel in granular material. *J Terramech*
  27. Das N (2007) Modeling three-dimensional shape of sand grains using discrete element method. PhD thesis, University of Florida
  28. Li W, Huang Y, Cui Y, Dong S, Wang J (2010) Trafficability analysis of lunar mare terrain by means of the discrete element method for wheeled rover locomotion. *J Terramech* 47(3):161–172
  29. Oda M, Iwashita K (2000) Study on couple stress and shear band development in granular media based on numerical simulation analyses. *Int J Eng Sci* 38:1713–1740
  30. Plassiard J-P, Belheine N, Donze F-V (2007) Calibration procedure for spherical discrete elements using a local moment law. Technical report, Universität Grenoble
  31. van der Linde J (2007) Discrete element modeling of a vibratory subsoiler. Master's thesis, University of Stellenbosch, Department of Mechanical and Mechatronic Engineering
  32. Asaf Z, Rubinstein D, Shmulevich I (2006) Evaluation of link-track performances using dem. *J Terramech* 43(2):141–161
  33. Harada T, Tanaka M, Koshizuka S, Kawaguchi Y (2007) Real-time coupling of fluids and rigid bodies. In APCOM, Kyoto
  34. Li A, Melanz D, Serban R, Negrut D (2014) A gpu-based preconditioned newton-krylov solver for flexible multibody dynamics. In: 3rd joint international conference on multibody system dynamics, IMSD 2014, Busan, Korea
  35. Negrut D, Tasora A, Anitescu M, Mazhar H (2011) Solving large multi-body dynamics problems on the GPU. In: GPU Gems, pp 269–280
  36. Kleinert J, Obermayr M, Balzer M (2013) Modeling of large scale granular systems using the discrete element method and the non-smooth contact dynamics method: a comparison. In: ECCOMAS multibody dynamics pp 1–4 July, University of Zagreb, Kroatien

37. Melanz D, Mazhar H, Negrut D (2014) Gauging military vehicle mobility through many-body dynamics simulation. In: The 3rd joint international conference on multibody system dynamics (IMSD 2014), Busan, Korea
38. Fleissner F (2012) Dokumentation, template-files und beispiele zum programmpaket "pasi-modo". Inpartik & Universität Stuttgart, Template files
39. Lichtenheldt R, Schäfer B (2013) Planetary rover locomotion on soft granular soils - efficient adaption of the rolling behaviour of nonspherical grains for discrete element simulations. In: 3rd international conference on particle-based methods, pp 807–818, ISBN 978-84-941531-8-1, Stuttgart
40. Lichtenheldt R (2015) A novel systematic method to estimate the contact parameters of particles in discrete element simulations of soil. In: 4th international conference on particle-based methods - particles 2015, pp 430-441, ISBN 978-84-944244-7-2, Barcelona
41. Lichtenheldt R, Schäfer B (2013) Planetary rover locomotion on soft granular Soils—efficient adaption of the rolling behaviour of nonspherical grains for discrete element simulations. In: 3rd international conference on particle-based methods, pp 807–818, ISBN 978-84-941531-8-1, Stuttgart, Germany
42. Lichtenheldt R, Schäfer B, Olaf K (2014) Hammering beneath the surface of mars—modeling and simulation of the impact-driven locomotion of the HP3-Mole by coupling enhanced multi-body dynamics and discrete element method. In: 58th Ilmenau scientific colloquium (IWK), Ilmenau, Germany, Technische Universität Ilmenau
43. Lichtenheldt R, Schäfer B (2013) Locomotion on soft granular soils: a discrete element based approach for simulations in planetary exploration. In: 12th symposium on advanced space technologies in robotics and automation: ASTRA 2013, Noordwijk, the Netherlands
44. Barnerdt WB et al. (2013) Insight: a discovery mission to explore the interior of mars. In: 44th lunar and planetary science conference, Texas, USA
45. Spohn T, Grott M, Smrekar S, Krause C, Hudson TL (2014) Measuring the martian heat flow using the heat flow and physical properties package (hp3). In: 45th lunar and planetary science conference
46. Lichtenheldt R (2015) Hammering beneath the surface of Mars—Analyse des Schlagzyklus und der äußeren Form des HP3-Mole mit Hilfe der Diskrete Elemente Methode. In: IFToMM D-A-CH 2015, Dortmund, Germany ISBN 978-3-940402-03-5
47. Lichtenheldt R, Schäfer B (2013) Locomotion on soft granular soils: a discrete element based approach for simulations in planetary exploration. In: 12th symposium on advanced space technologies in robotics and automation, ESA/ESTEC, Netherlands
48. Wedler A, Rebele B, Reill J, Suppa M, Hirschmüller H, Brand C, Schuster M, Vodermayr B, Gmeiner H, Maier A, Willberg B, Busmann K, Wappler F, Hellerer M, Lichtenheldt R (2015) LRU - lightweight rover unit. In Proceedings of the 13th symposium on advanced space technologies in robotics and automation (ASTRA)
49. Wedler A, Hellerer M, Rebele B, Gmeiner H, Vodermayr B, Bellmann T, Barthelmes S, Lange C, Witte L, Schmitz N, Knapmeyer M, Czeluschke A, Thomsen L, Waldmann C, Wilde M, Takei Y (2015) Robex components and methods for the planetary exploration demonstration mission (1). In: 13th symposium on advanced space 820 technologies in robotics and automation, ESA/ESTEC, Netherlands
50. Apfelbeck M, Kuß S, Rebele B, Schäfer B (2011) A systematic approach to reliably characterize soils based on bevameter testing. *J Terramech Elsevier* 48:360–371
51. Dahlquist G (1963) A special stability problem for linear multistep methods. *BIT* 3(1):27–43
52. Lichtenheldt R, Schäfer B, Krömer O, van Zoest T (2014) Hammering beneath the surface of Mars - forensic engineering of failures in the HP3-Mole by applying multi-body dynamics simulation. In: Proceedings of 3rd international conference on multibody system dynamics IMSD 2014, ISBN 978-89-950027-7-3, Busan, Korea